

Unstable behavior of anodic arc discharge for synthesis of nanomaterials

Sophia Gershman and Yevgeny Raitses

Princeton Plasma Physics Laboratory, Princeton, NJ 08543, USA

E-mail: sgershma@pppl.gov

Received 5 December 2015, revised 19 June 2016

Accepted for publication 27 June 2016

Published 27 July 2016



Abstract

A short carbon arc operating with a high ablation rate of the graphite anode exhibits a combined motion of the arc and the arc attachment to the anode. A characteristic time scale of this motion is in a 10^{-3} s range. The arc exhibits a negative differential resistance before the arc motion occurs. Thermal processes in the arc plasma region interacting with the ablating anode are considered as possible causes of this unstable arc behavior. It is also hypothesized that the arc motion could potentially cause mixing of the various nanoparticles synthesized in the arc in the high ablation regime.

Keywords: plasma instabilities, arc discharge, arc instabilities, atmospheric pressure arc, nano materials, nanotubes, arc synthesis

(Some figures may appear in colour only in the online journal)

1. Introduction

A carbon arc discharge with a consumable anode (so-called anodic arc) is widely used for synthesis of carbon nanomaterials [1–3]. A typical arc setup consists of a graphite anode and a cathode made either from graphite or a metal [4, 5]. The heating by the arc causes intense evaporation of the anode and a portion of the ablated anode material is deposited on the cathode. The arc operates in an atmosphere of buffer gas, usually helium, but the plasma in the anodic arc with a graphite anode consists mainly from the evaporated carbon products. For the synthesis of fullerenes, the buffer gas pressure does not exceed 100–200 torr [6, 7]. The arcs operating at higher pressures of about 500–600 torr are used for synthesis of multi-walled carbon nanotubes (MWNTs) [1, 2]. With the addition of metal catalysts, the atmospheric pressure carbon arcs can produce single wall nanotubes (SWNTs) [3]. Moreover, with the application of an external magnetic field, the arc discharge can produce graphene flakes [7]. For all these synthesis applications, the arc is usually operated in a current limited regime and the arc voltage is controlled by maintaining a constant gap of a few millimeters between the arc electrodes.

In spite of a wide use of short anodic arcs for synthesis applications, the arc operation in the presence of a strong anode ablation is not well understood. For example, in recent studies [4, 5, 8], we showed that for the arc with a graphite anode at a given arc current, there is a critical anode diameter larger than which, the ablation rate remains nearly constant with the anode diameter. For smaller anode diameters, the ablation rate increases much faster than it could be expected from the increase of the current density at the anode. A majority of the synthesis arc processes are implemented in this particular ablation regime. These arcs are known for a high yield production of nanotubes in volume, but with a very poor selectivity [9]. The characteristics of the produced nanotubes (e.g. size, aspect ratio) depend on the plasma parameters and on the nanotube residence time in the synthesis region [10–13]. In addition, during the arc operation, nanoparticles of different dimensions and structures can be produced including nanotubes, fullerenes and carbon nanoparticles etc. Hence, the arc stability can be important to maintain steady state generation of the charged and neutral particles and fluxes and heat fluxes involved in the synthesis processes, including nucleation and growth of nanoparticles and nanostructures [9, 12]. In this paper, we show that a typical carbon arc with a consumed anode used for synthesis of carbon nanotubes is highly

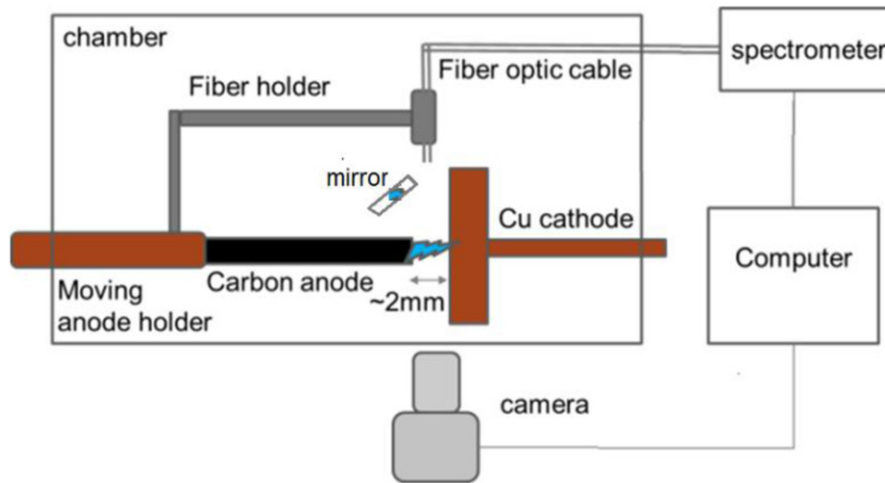


Figure 1. The diagram of the experimental setup shows the He filled chamber (500 torr), carbon anode—copper and cathode, the camera, and the spectrophotometer arrangements.

Optical Emission Spectrum Showing the C Swan Bands

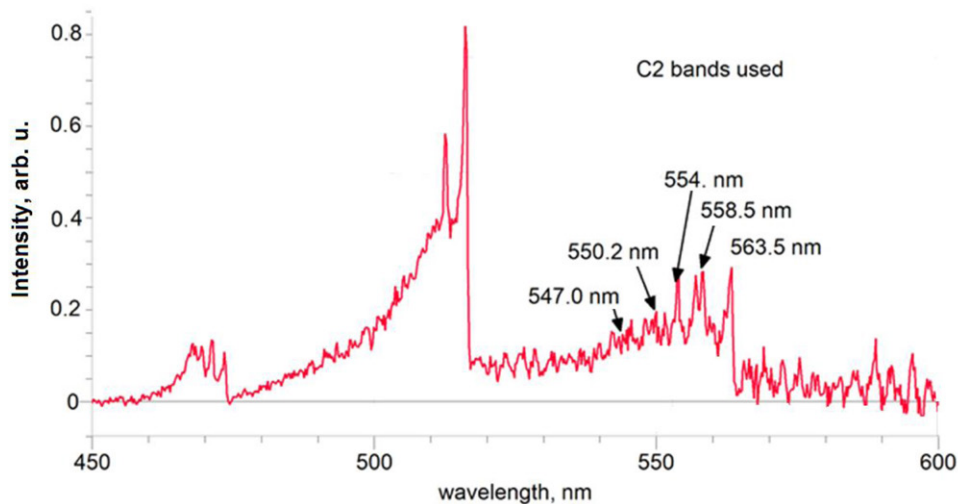


Figure 2. A section of the OES spectrum of the arc. The spectrum shows the 563.5 nm $A^3\Pi_g - X^3\Pi_u \Delta\nu = +1$ transitions used to determine the vibrational excitation temperature.

unstable. The observed instability may contribute to mixing of nanoparticles causing a poor selectivity of the arc synthesis.

The arc instabilities that involve anode processes have been investigated for the low current (<5 A) high pressure arcs used in high intensity lighting devices and atmospheric pressure plasma torches [14–17]. Experimental studies show current and voltage oscillations correlated with the anode arc attachment phenomena such as the displacement of the arc root and with the variations in the types of arc anode attachments from the diffuse to constricted or multiple attachments. Theoretical modeling efforts reveal the importance of including a region of the plasma column in the arc unstable behavior. According to [18], 3D models lead to unstable behaviors because they take into account the significant gradients exist in the arc plasma properties, the anode surface properties, and the gas properties and fluxes [18]. However, the existing 3D models do not take into account the high anode ablation or the resulting high gas and particle flows from the anode. Additional studies are

needed for the medium currents (50–100 A) and short gaps relevant to the anodic arc used for the synthesis of nanomaterials. In this paper, we propose a simplified model for the observed arc unstable behavior and consider some additional specific types of instabilities in the appendix.

2. Experimental methods

The experiments were conducted using a carbon arc setup (figure 1) described elsewhere [4, 5, 8]. This setup consists of a graphite anode and a copper cathode. In the described experiments, the cathode diameter was 5 cm and the anode diameter was varied from 0.3–1.2 cm. The discharge current was kept constant of 65 A. Depending on the anode diameter, the discharge voltage was 20–30 V. This voltage includes the voltage drop across the electrodes and the arc discharge. The arc was operated with a helium buffer gas at a pressure of 500 torr.

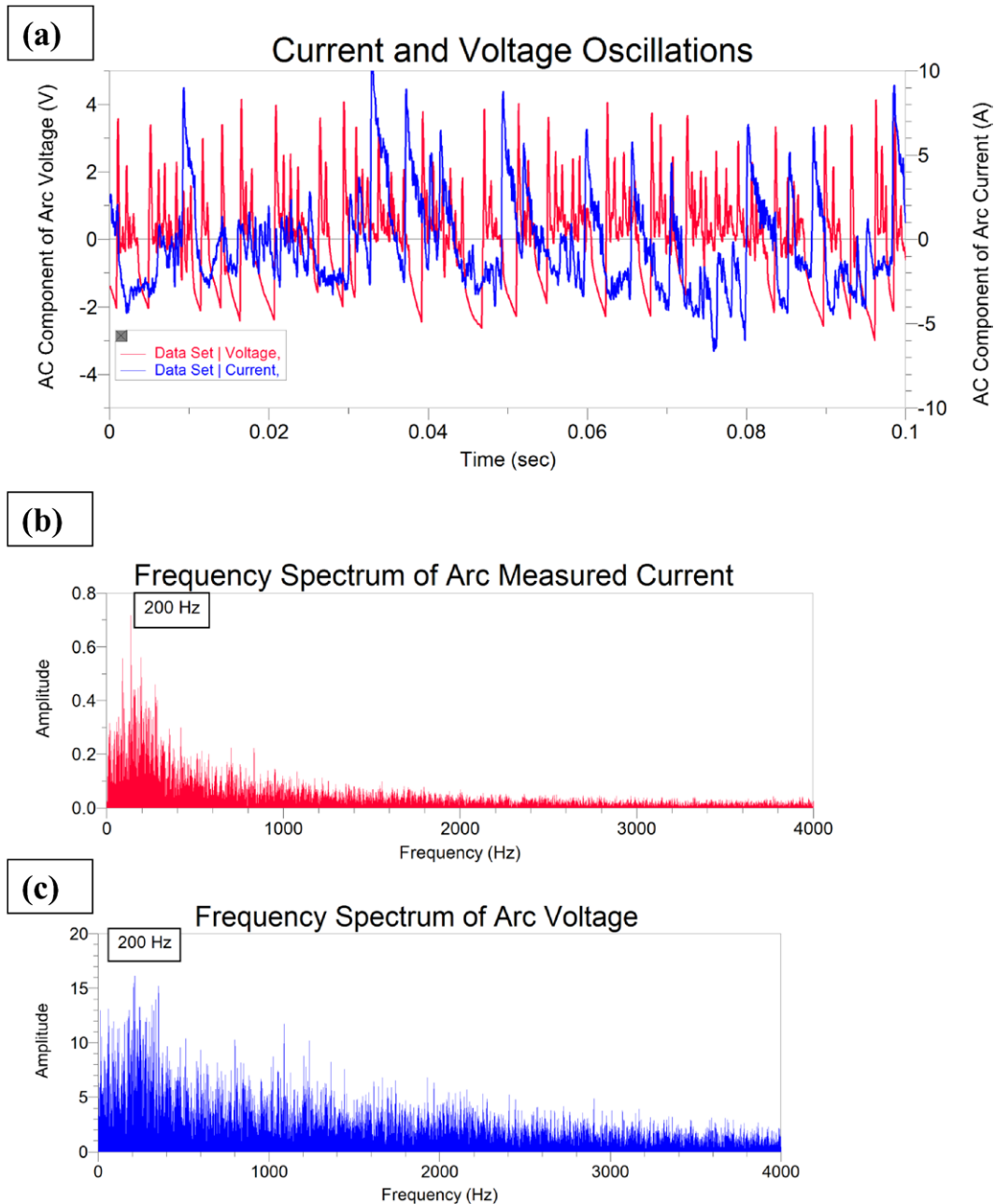


Figure 3. Current and voltage oscillograms for an arc with a 6 mm anode (a) and the corresponding FFT results (b) and (c) showing the peak frequencies of about 200 Hz. AC coupling was used for these measurements. The arc settings were 27–32 V and 65 A.

During the arc operation, a cathode deposit is usually formed. This deposit serves as the actual cathode [4, 5]. The arc is initiated with the electrodes in contact with each other and the anode is then moved away from the cathode by a stepper motor. In the present experiments, the distance between the anode and the cathode deposit is maintained constant by moving the anode relative to the stationary cathode as the anode ablates. The position of the anode is controlled by maintaining the set voltage between the electrodes using a Labview feedback loop. In a separate set of arc experiments with cathodes made from copper and graphite, it was confirmed that because of the formation of the cathode deposit, the arc operation is not sensitive to the cathode material. All measurements were taken 20–30 s after the arc ignition at a

stable inter-electrode distance and all experimental conditions were repeated for consistency.

Synchronized electrical and optical emission spectroscopy (OES) measurements, and high speed imaging were used to investigate the arc operation. The spectra were measured using an OceanOptics HR4000 spectrophotometer with 1 ms exposure and 1000 Hz repetition rate. Fast imaging was conducted using a Photronix FastCam video camera at 10 000–50 000 frames per second. Images were taken with a combination of an infrared cut-off and a 470 ± 10 nm band pass filters. Each fast imaging sequence was about 2 s in duration taken approximately 30 s after the start of the arc. A mirror was placed behind the arc in such a way that the camera recorded the arc and its reflection at

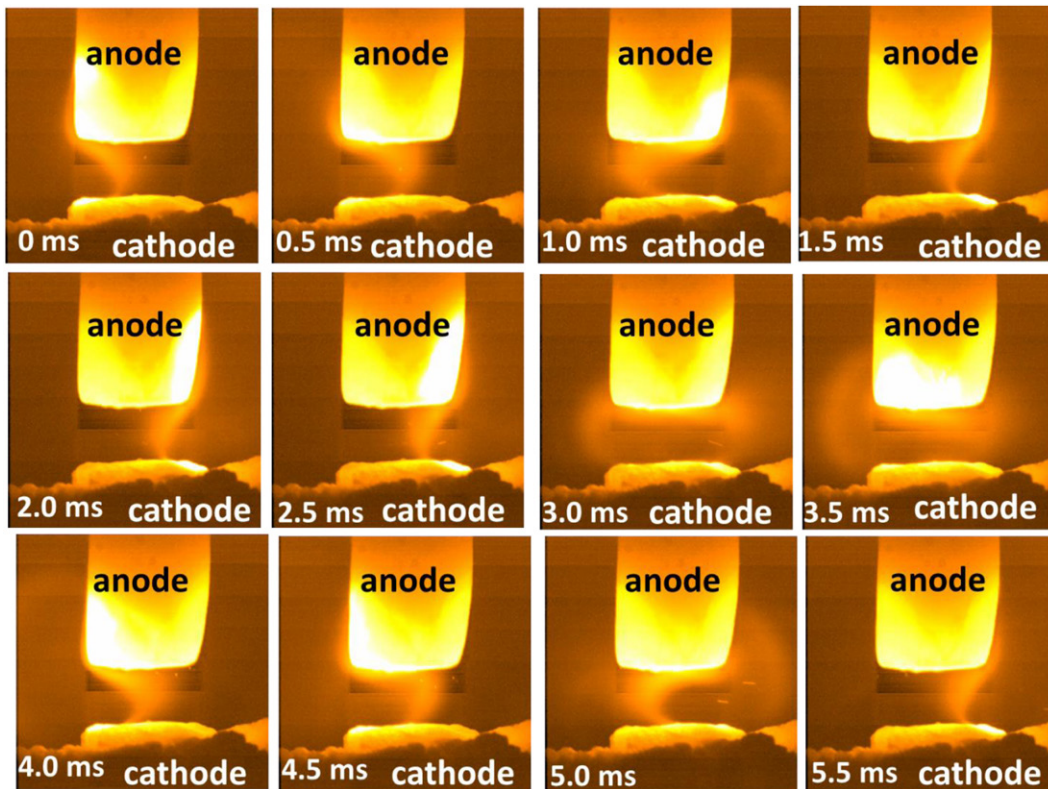


Figure 4. Snapshots, 0.5 ms apart, from a 10000 frames per second fast imaging of an arc with a 6 mm anode. The snapshots show the curved arc column and the anode hot region moving around the anode.

the same time (figure 1). Voltage and current measurements were taken using a Lecroy digital storage oscilloscope, and the current was measured across a 2 m Ω shunt resistor. The fast camera and the oscilloscope measurements were synchronized using a National Instruments Data Acquisition system.

3. Experimental results

The OES measurements confirmed that after the ignition process is completed, the arc burns primarily in carbon gas, as evident from the presence of C and C⁺ lines and C₂ and C₃ bands and a conspicuous absence of He lines. The electron excitation temperature was calculated assuming a local thermal equilibrium (LTE) and using Boltzmann plots for the C₂ Swan band intensities (figure 2) [19–22]. The vibrational excitation temperature was determined to be 1.0 \pm 0.2 eV. The gas temperature was estimated by fitting the continuum part of the spectra and using the Wien's Displacement law to find the arc temperature. This method gave the temperature in the range of 4500–5000 K [23]. These values agree with the ~4500 K rotational temperature determined by fitting the rotational structure of the 519 nm C₂ Swan band [17]. The results of OES measurements are used below for energy calculations in the arc plasma.

Even after the transient phase of the ignition, the arc exhibits unstable behavior that includes both arc current oscillations and the movement of the arc column and the anode attachment region. This unstable behavior of a short anodic arc

with high anode ablation has been characterized and reported here for the first time. We found a correlation between discharge current and voltage oscillations and the arc movement. In particular, current and voltage measurements revealed non-stationary oscillations of 20% of the current amplitude and 10% of the voltage amplitude, both at frequencies of 200–300 Hz as shown in figure 3. The high speed imaging revealed that the curved bright arc region is moving together with the bright anode region. For example, figure 4 shows single frames, 0.5 ms apart, selected from 10000 frames per second imaging of an arc with a 0.6 cm diameter anode. These images show the curved arc column and the hot anode region moving together around the anode. Comparing the images of the anode side facing the anode with the simultaneous images of reflected image of the back of the anode, we confirmed the movement of the arc and the hot attachment region all the way around the anode.

ImageJ particle tracking and edge tracking functions were used to analyze the movement of the arc column and the anode bright region. These methods generate a plot of the position of the arc column and the anode hot region as functions of time revealing oscillations with a frequency of 200–300 Hz (figure 5) and the speed of the arc column motion in the range of 10 m s⁻¹ for the 0.6 cm anode. Thus, the fast imaging and the synchronized current measurements reveal the same frequency of oscillations (figures 5 and 6). Isolating the movement of the anode hot region shows gradual movement in a direction that is somewhat random. The speed of the movement of the boundary of the anode hot region determined by the edge tracking method is also in the range of

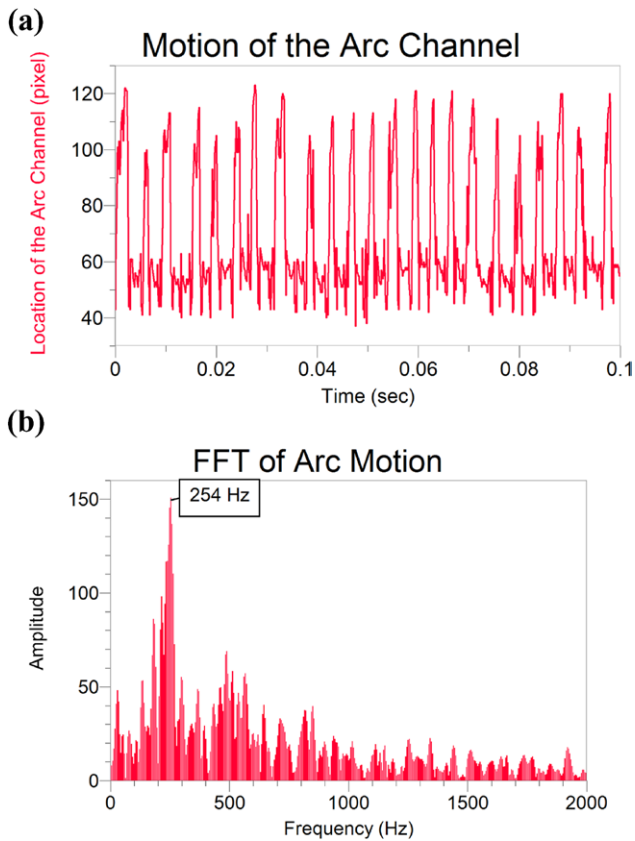


Figure 5. The positions of the arc channel in each frame from the 10000 fps imaging of an arc with a 6 mm anode. (a) Shows the positions at various times and (b) shows the fast Fourier transform showing the dominant frequency of the arc motion (254 Hz).

10 m s^{-1} (figure 7). In addition, videos also show the flow of material from the anode to the cathode at speeds in the range of $1\text{--}10 \text{ m s}^{-1}$. This motion has been confirmed in repeated experiments in the high ablation mode observed for the 0.6 cm anode and 65 A current. Higher frequencies may be present with lower ablation for larger anode diameters or lower currents.

4. Discussion

Investigations of arc instabilities have a long history and include arcs with currents ranging from milli-amperes to thousands of amperes and pressures from high pressure to vacuum, arcs with various carrying gasses, flowing and stationary. The instabilities include variations in current and voltage as well as the movement of the arc. The mechanisms developed to understand this behavior include the influence of the self-magnetic field, the influence of the heat balance in the arc, the interactions of the arc with the cathode and/or the anode [14, 24–28, 31–33]. In the present experiments, we observed a complex arc behavior including periodic and random components and involving the arc column and the anode. This behavior was not explained in previous studies because short anodic arcs were not well investigated and diagnosed in the past. We analyzed a number of typical arc instabilities driven by different mechanisms including electromagnetic, convection and

thermal mechanisms [24–29]. Their brief analysis is given in appendix. We propose the negative differential resistance combined with a thermal mechanism as responsible for the observed unstable behavior of the carbon arc. These considerations are based on the analysis of the electrical signal of the arc and on the comparison of the characteristic time scales of our experimental observations with time scales of the physical processes involved in some of these instabilities.

The process of heating, sublimation, and movement of the anode hot region can be divided into two phases. During the first phase, the heat supplied to the anode is balanced by the heat needed to increase the temperature of the anode attachment region to the sublimation temperature. During the second phase, the sublimation of the anode material leads to the cooling of the arc core and the movement of the arc. The speed of this movement is limited by the time it takes to heat a region of the anode to sublimation temperature.

4.1. Physical mechanism of arc unstable behavior

The proposed physical mechanism of the observed motion of the arc is shown in figure 8. The plasma current heats the anode and leads to the sublimation of the anode material. The influx of low energy carbon vapor into the plasma reduces the conductivity in this region and hence the current density,

$$j = \sigma(T) \left(E + \frac{k_B T_e}{n_e} \frac{dn_e}{dz} \right), \quad (1)$$

where $\sigma(T)$ is the plasma conductivity as a function of plasma temperature, E is the electric field in the plasma column, and the second term is the diffusion component of the current. To determine the reasons for the decrease in the current density a full model of the plasma-electrode system is needed, which is beyond the scope of this paper. The reasons may include the reduction in the anode potential, the increase is the electron and ion collision rates with the influx of neutral particles due to the high ablation, and the decrease in the plasma temperature [25]. The observed 20% reduction in the plasma current (figure 3(a)) implies that the arc column moves without interruption in the discharge (at the time resolution of this experiment). As the current density in the center of the plasma decreases, the current density and the heat flux become higher in the outside region of the plasma channel and heat the surface of the anode in this region. The peripheral region then becomes the new center of the plasma channel due to the expansion of the channel. The result is the movement of the anode hot region and the arc channel (figure 8). For the motion to occur, the time to restore the current in the original location should be longer than the time to increase the current in the new location. The lower conductivity in the original region means that to restore the current, either the voltage needs to increase or the gap between the electrodes needs to decrease. Recall that in our setup, the voltage is controlled by the stepper motor via a negative feedback. This stepper motor is too slow to respond to the 200–300 Hz oscillations in voltage (figure 3). The fast frame camera recorded no changes in the arc gap during the arc oscillations. Hence, the arc voltage and thereby,

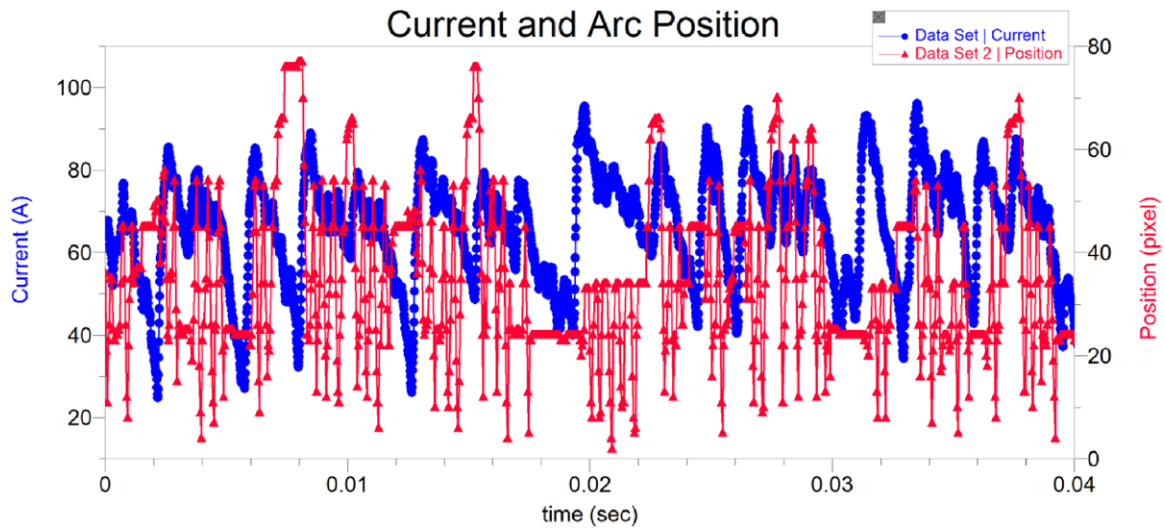


Figure 6. Positions of the arc channel correlated with the current oscillations. The camera frame rate was 25 000 fps. The positions of the arc channel were recorded using the ImageJ software. The current was measured across a 2 mΩ shunt resistor.

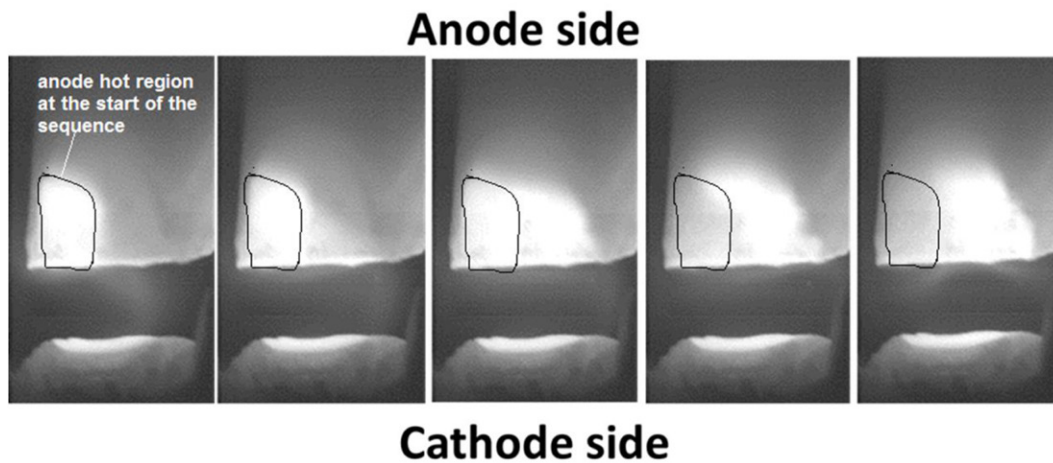


Figure 7. Consecutive images of the anode hot region taken at 25 000 frames per second, 4×10^{-4} s exposure time. The images are taken for a 6 mm anode. The images show the carbonaceous deposit on the cathode. The distance between the deposit and the anode is 2 mm. The arc column is dim in these images due to the choice of filters.

the arc current cannot be restored fast enough in the original location. The current continues to flow in the region of the arc adjacent to the cooled column and heats the plasma and the anode surface. This is certainly a simplified description of the arc oscillations, but it may explain the voltage and current oscillations measured in the arc discharge. It can be deduced from measured traces of figure 3 that in these oscillations arc demonstrates a negative differential resistance, $dV/dI < 0$ (~ -50 mΩ) before the current reaches its maximum value (and presumably, maximum ablation), while the voltage drops to the minimum. After that, the arc is recovered restoring both the voltage and the current (figure 3(a)). Oscillations of both the arc current and the arc voltage have a similar type of the spectrum (figures 3(b) and (c)) with a characteristic rise time on the order of 0.1 ms.

In addition to the existence of a negative differential resistance, the proposed mechanism of the arc movement is supported by our estimations showing that the time to heat the new region of the anode matches the time scale of the arc

movement observed in our experiments. For these estimations, we adopt the approach used in the estimates of the thermal ablation of rocket nozzles as in [29]. If the arc moves continually around an anode of a radius, r , at a speed, v , then the maximum time each point of the anode is exposed to the heat flux from the plasma, is

$$t = \frac{2\pi r}{v}, \quad (2)$$

which for the anode diameter of 0.6 cm and the measured speed of 10 m s^{-1} , is about 2 ms. If the proposed model fits the experimental observations then this time should be sufficient to heat the anode attachment region to the graphite sublimation temperature. To find this time, we calculate the evolution of the anode surface temperature at a point inside the arc attachment region. The process of heating, sublimation, and movement of the anode hot region can be divided into two stages. During the first stage, the heat supplied to the anode is balanced by the heat needed to increase the temperature of the

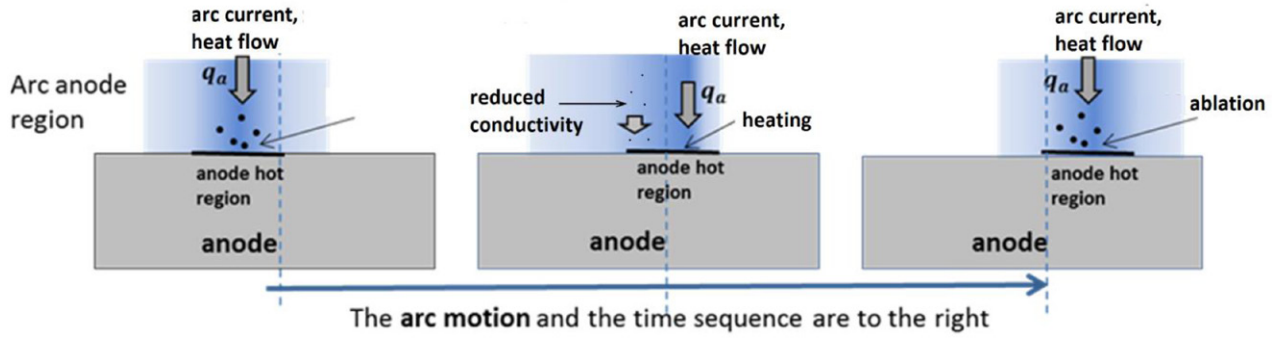


Figure 8. The diagram of the mechanism of the arc movement. The diagram shows the side view of the anode-plasma region with high intensity heating and ablation in the center, followed by the decrease in the energy flux to the surface in the center region and heating in the peripheral region, and resulting in the movement of the arc and anode attachment region. As the conductivity of the original arc column decreases, the voltage provided by the outside source remains the same. The figures show a time sequence of the arc movement from left to right.

anode attachment region to the sublimation temperature. This problem can be formulated as a one dimensional heating of an infinite slab if the Fourier number is much smaller than unity. The Fourier number is the ratio of heat conduction to storage, and a small Fourier number implies that the heated surface region is very thin compared to the size of the slab [30, 35]. The maximum Fourier number is

$$F = \frac{\delta t}{d^2}, \quad (3)$$

where $\delta = 1.3 \cdot 10^{-2} \text{cm}^2 \text{s}^{-1}$, is thermal diffusivity for graphite at high temperatures [29] and $d \approx 0.2 \text{cm}$, is the diameter of the heated region. These values give $F \leq 10^{-3}$ which means that we can consider the anode heating as a 1D heat diffusion problem, in z -direction only. The solution gives the temperature at a point and time, (z, t) , which in turn gives the time for the anode at an initial temperature T_a , to reach the sublimation temperature, T_s :

$$t = \frac{\pi k (T_s - T_a)^2}{4 \delta \dot{q}^2}, \quad (4)$$

To evaluate this time, we need to estimate the rate of heat flux to the surface of the anode. Assuming a Maxwellian electron energy distribution, the added energy flux rate to the anode,

$$\dot{q}_a = J(2k_B T_e + V_a), \quad (5)$$

Where J —is the plasma current, $T_e = 1 \text{eV}$, is the electron temperature, and V_a is the anode potential. Recent simulations have shown that the anode potential is positive for the short anodic arc with high ablation [11]. According to [11], the volt-equivalent of the heat flux is $V_{\text{eff}} \approx 10.7 \text{V}$, and

$$\dot{q}_a \approx \frac{I_{\text{arc}} V_{\text{eff}}}{\text{area}}, \quad (6)$$

where, $I_{\text{arc}} = 65 \text{A}$, from the experiment, and the area is assumed to be the anode attachment region. This area was estimated from the images of the anode to be about 0.1cm^2 so the current density is about 650A cm^{-2} . Hence, the estimated heat flux is $\dot{q}_a \approx 7 \times 10^3 \text{W cm}^{-2}$. The remaining quantities in equation (4) are the thermal conductivity of graphite

at high temperature, $k = 40 \text{W mK}^{-1}$ and the temperature change, $T_s - T_a$. The sublimation temperature of graphite is, $T_s \approx 3700 \text{K}$, and $T_a \sim 3200 \text{K}$ from the previous IR measurements [5, 36]. This gives the heating time $t \approx 2 \text{ms}$. This time agrees with the estimates (above) based on the observed motion of the anode attachment region. Under such conditions, a 0.2cm diameter arc attachment to the anode passes around a 0.6cm anode at a frequency of about $100\text{--}300 \text{Hz}$. The frequencies obtained from the fast imaging results fall in this range. This is the slowest of the considered processes involved in the interactions of the plasma with the anode and as such it is going to dominate the arc motion. Hence, we suggest that the anode heating is a likely the process which governs the characteristic time of the motion of the arc attachment to the anode.

4.2. Energy balance in the plasma-anode region

The energy balance in the plasma—anode region, the region of the arc column that interacts with the anode surface, is as follows. The energy added to the plasma-anode region, \dot{q}_a , is given by equation (5) above, and the energy removed from the region is

$$\dot{q}_r = \Gamma_C [H_v + 2k_B T_C + \alpha E_i + \alpha 2k_B T_i] + \Phi_{\text{rad}} + \varepsilon \sigma T_a^4 + \kappa \frac{\Delta T}{\Delta x}. \quad (7)$$

The energy removed includes the energy losses due to the sublimation of graphite, the energy lost to radiation emitted by the plasma column, the energy lost to radiation emitted by the hot anode, and the energy conducted by the anode material. Here, Γ_C is the carbon vapor flux due to ablation, $H_v \approx 7.3 \text{eV}$ is the heat of vaporization (per particle) for graphite at high temperature [34, 35, 36], $T_C \approx 4500\text{--}5000 \text{K}$ is the gas temperature measured using OES, α is the degree of ionization, $E_i = 11.2 \text{eV}$ is Carbon first ionization energy, T_i is the ion temperature in the plasma, ε is emissivity of graphite, σ is the Stephan–Boltzmann constant, T_a is the temperature of the anode, and κ is the thermal conductivity of graphite.

Numerical estimates of equation (7) show that the energy losses are dominated by the heat of vaporization with some contribution from the anode cooling processes. Assuming local thermal equilibrium, Saha equation for $T_e \approx 10\,000\text{ K}$ gives the degree of ionization $\alpha \approx 0.1\%$. This low degree of ionization makes the contributions of ionization and heating of the ionized material insignificant compared to the heat of vaporization and heating of the neutral atoms. The energy lost to radiation is not significant for T_e less than about 2 eV and hence can be neglected here. The anode cooling has been computed previously and contributes approximately 0.1 of the energy lost to evaporation [4, 5]. Hence, the energy removed can be simplified to

$$\dot{q}_r = \Gamma_C [H_v + 2k_B T_C] + \Phi, \quad (8)$$

Here Φ includes all contributions that add up to about 0.1 of the first term. The ablation rate was measured previously to be about 10 mg s^{-1} [4, 5]. Using the 0.10 cm^2 measured anode attachment region as the ablating area, gives the particle flux, $\Gamma_C \approx 5 \times 10^{21}\text{ cm}^{-2}\text{ s}^{-1}$. Then $\dot{q}_r \approx 6.6 \times 10^3\text{ W cm}^{-2}$, compared to the above, $\dot{q}_a \approx 7 \times 10^3\text{ W cm}^{-2}$. This means that after the anode surface reaches the sublimation temperature, the energy flux is balanced, and the anode hot region is maintained at constant temperature during the ablation process, provided the energy input doesn't change. The added energy, \dot{q}_a , is affected by the current density, plasma temperature, and the anode potential. The injection of the ablated material into the plasma-anode region decreases the added energy flux by affecting the current density and the anode potential. Models are currently being developed that describe these processes in greater detail.

4.3. Remarks on the effect of instabilities on the nanosynthesis

According to [12], the nucleation and growth of nanotubes occur in this peripheral region of the arc discharge. A typical time required for nucleation and growth of nanoparticles is limited by the residence time of nanoparticles in this plasma region. Following [12], the residence time is $\sim 2\text{ ms}$ that is comparable with characteristic time of the arc movement observed in our experiments. Thus, these arc oscillations perturbing the location of the synthesis region can affect the residence time of nanoparticles causing the mixing of nanoparticles of different sizes and structures. The implications for the selectivity of the nanoparticle production are important for the high ablation regime that is characterized by the arc oscillations in the 200–300 Hz range.

5. Conclusions

Fast imaging and electrical current measurements revealed unstable behavior of the carbon arc discharge for synthesis of nanomaterials. The arc column and the arc attachment region to the anode move in a somewhat sporadic way with a characteristic time of 2 ms. A physical mechanism is proposed based on the thermal processes in the arc plasma region

interacting with the ablating anode which leads to the shift of the arc to the new anode region. According to the transient heat transfer analysis, the time needed to heat the new anode region is $\sim 2\text{ ms}$. For a 0.6 cm diameter anode used in our experiments, this time scale yields a frequency of about 200–300 Hz that is comparable with the measured frequency of the arc motion. Our model suggests that the injection of the ablating material into the plasma locally reduces the energy flux to the surface and leads to the arc shifting to the adjacent position. This model is indirectly supported by the measured negative differential resistance of the arc discharge during the arc oscillations. A more detailed model of the anode processes is needed to fill in the details of this process.

Among practical implication of this study the observed unstable behavior of the arc discharge may be responsible for mixing of nanoparticles flow leading to a poor selectivity, which is typical for the arc synthesis method.

Acknowledgments

The authors wish to thank Drs Valerian Nemchinsky, Vlad Vekselman and Mikhail Shneider for fruitful discussions of the experimental results and to Mr Alex Merzhevskiy and Mr Yao-Wen Yeh for their assistance with experiments. The authors also wish to thank Drs Igor Kaganovich and Brent Stratton for fruitful discussions of this research. This work was supported by US Department of Energy, Office of Science, Basic Energy Sciences, Materials Sciences and Engineering Division.

Appendix

Here we discuss the roles of convection and the self-magnetic field in the unstable behavior of the anodic arc in the high ablation regime. The arched shape and the upward motion observed in the peripheral regions of the images prompted us to check the role of convection in the motion of the arc. Convection speed is of the order, $v_c = \sqrt{gL}$, where g is gravitational acceleration and L is a characteristic length. Assuming, L is on the order of the arc length, $\sim 0.2\text{--}0.4\text{ cm}$, the convection speed is expected to be about $10\text{--}20\text{ cm s}^{-1}$. Although some convection should be expected for the considered experimental conditions, it is too slow to fully account for the observed unstable behavior of the carbon arc. Moreover, a comparison of the arc operation with the electrodes in the horizontal and vertical positions showed no differences in arc oscillations.

Considerations were given also to the possibility of a 'kink' instability caused by the self-induced magnetic field of the arc, B_{self} . To evaluate the possibility of this instability we compared the magnetic field energy density input into the arc, $\frac{B_{\text{self}}^2}{2\mu_0}$, to the arc thermal energy density [31]. For our experimental conditions, the current density, J , is approximately $10^6\text{--}10^7\text{ A m}^{-2}$. Assuming the arc column radius on the order of 0.1 cm, $\frac{B_{\text{self}}^2}{2\mu_0} \approx 10\text{ J m}^{-3}$. This is a few orders of magnitude lower than the thermal energy density in the arc ($\sim 10^4\text{ J m}^{-3}$) [29, 30].

Thus, it is unlikely that the kink instability is responsible for the observed motion of the arc. Indeed, this instability is more likely to play a major role for large currents, long arcs, constricted attachments, or in the presence of outside magnetic fields [31]. The typical frequency range of the ‘kink’ instability is in the kilohertz range. This is much faster than the observed frequency of the arc motion. Another possibility is that due to the arc curvature, $J \times B_{\text{self}}$, causes a ‘firehose’ type of instability. In this case, the resulting arc rotation would be also an order of magnitude faster than the observed frequency [28, 31].

Note that [13] suggested that fast anode jets affect the behavior of the arc column. According to this modeling study, the fast jet ($\sim 100 \text{ m s}^{-1}$) forms in the powdered center of a graphite anode used for the synthesis of single wall nanotubes. However, our fast imaging measurements showed no fast jets at the anode. We observed particles of $>50 \mu\text{m}$ moving at speeds of $5\text{--}20 \text{ m s}^{-1}$ several times slower than 100 m s^{-1} . In addition, from imaging measurements, the anode attachment has a diffuse form, while the fast anode jets are usually formed by a constricted anode spot.

References

- [1] Iijima S 1991 *Nature* **354** 56–8
- [2] Ebbesen T W and Ajayan P M 1992 *Nature* **358** 220–2
- [3] Journet A, Maser W K, Bernier P, Loiseau A, Lamy de la Chapelle M, Lefrant S, Denlard P, Lee R and Fischer J E 1997 *Nature* **388** 756
- [4] Ng J and Raitses Y 2014 *Carbon* **10** 80–8
- [5] Ng J and Raitses Y 2015 *J. Appl. Phys.* **117** 063303
- [6] Afanas’ev D V *et al* 1997 *Tech. Phys.* **42** 234
- [7] Volotskova O, Levchenko I, Shashurin A, Raitses Y, Ostrikov K and Keidar M 2010 *Nanoscale* **2** 2281–5
- [8] Fetterman J *et al* 2008 *Carbon* **46** 1322–6
- [9] Prasek J *et al* 2011 *J. Mater. Chem.* **21** 15872
- [10] Shashurin A and Keidar M 2008 *Carbon* **46** 1792–828
- [11] Nemchinsky V A and Raitses Y 2015 *J. Phys. D: Appl. Phys.* **48** 245202
- [12] Keidar M 2007 *J. Phys. D: Appl. Phys.* **40** 2388–93
- [13] Kundrapu M, Li L, Shashurin A and Keidar M 2012 *J. Phys. D: Appl. Phys.* **45** 315305
- [14] Yang G and Heberlein J 2007 *Plasma Sources Sci. Technol.* **16** 765–73
- [15] Mentel J and Heberlein J 2010 *J. Phys. D: Appl. Phys.* **43** 023002
- [16] Benilov M 2008 *J. Phys. D: Appl. Phys.* **41** 144001
- [17] Ghorui S *et al* 2007 *Phys. Rev. E* **76** 016404
- [18] Trelles J 2013 *Plasma Sources Sci. Technol.* **22** 025017
- [19] Pearse R W B and Gaydon A G 1976 *The Identification of Molecular Spectra* 4th edn (New York: Wiley)
- [20] Herzberg G 1950 *Spectra of Diatomic Molecules I* 2nd edn (New York: VNR)
- [21] Harilal S S *et al* 1997 *J. Phys. D: Appl. Phys.* **30** 1703–9
- [22] Brooke J S A *et al* 2013 *J. Quant. Spectrosc. Radiat. Transfer* **124** 11–20
- [23] Mirapeix J 2008 *J. Phys. D: Appl. Phys.* **41** 135202
- [24] Lehnert B 1967 Experimental evidence of plasma instabilities *Plasma Phys.* **9** 301–37
- [25] Nemova T N and Stepanov A P 2014 *Weld. Int.* **28** 631–5
- [26] Karasik M and Zweben S J 2000 *Phys. Plasmas* **7** 4326–40
- [27] Liang F, Tanaka M, Choi S and Watanabe T 2014 *J. Phys.: Conf. Ser.* **518** 012027
- [28] Zhang J L, Yan J D and Fang M T C 2004 *IEEE Trans. Plasma Sci.* **32** 1352
- [29] Marotta A and Sharakhovsky L I 1996 *J. Phys. D: Appl. Phys.* **29** 2395–403
- [30] Cengel Y A and Ghajar A J 2014 *Heat and Mass Transfer—Fundamentals and Applications* 5th edn (New York: McGraw-Hill)
- [31] Mentel J 2009 The magnetic instability of arcs *The Electric Arc* ed H Maecker *et al* (Herausgeber: H. Popp Matlab GmbH, D 82335 Berg)
- [32] Nemchinsky V 2014 *IEEE Trans. Plasma Sci.* **42** 4026–30
- [33] Boulos M I, Frauchais P and Pfender E 1994 *Thermal Plasmas: Fundamentals and Applications* vol 1 (New York: Plenum)
- [34] Clarke J T and Fox B R 1969 *J. Chem. Phys.* **51** 3231
- [35] Gebhart B 1971 *Heat Transfer* 2nd edn (New York: McGraw-Hill)
- [36] Yeh Y, Raitses Y and Yao N 2016 *Carbon* **105** 490–5